PROCEEDINGS OF SCIENCE

A possible effect of the Fermi bubbles and associated magnetic structures on the incoming directions of Ultra-High Energy Cosmic Rays

Thomas Fitoussi,[a,*] **Gustavo Medina-Tanco**[b] **and Juan Carlos D'Olivo**[b]

[a] *Karlsruhe Institute of Technology, Institute for Astroparticle Physics, Karlsruhe, Germany*

[b] *Instituto de Ciencias Nucleares, UNAM, Circuito Exteriror S/N, Ciudad Universitaria, 0.210 Ciudad de México, CDMX, Mexico*

E-mail: thomas.fitoussi@kit.edu, gmtanco@nucleares.unam.mx, dolivo@nucleares.unam.mx

There are numerous indications that the Milky Way has a hot material outflow originating from the Galactic center. Among others, the so-called Fermi bubbles discovered in 2010 strengthens this possibility. The origin of this nuclear wind is still disputed, either the episodic activity of Sagittarius A*, the supermassive black hole at the Galactic center, or a nuclear start burst in its vicinity have been invoked as possible powering sources. In any case, these symmetrical structures, already observed in both gamma-rays, X-rays, and radio, show evidence of a hot magnetized coronal phase entrained by molecular clouds. Moreover, radio polarization measurements evidence the presence of structured magnetic fields in the general perpendicular direction to the central Galactic plane. Indeed, magnetohydrodynamic simulations point to the possible existence of a well-structured field reaching as high as 15 kpc or more above the energy input region in the plane, with intensities on the order of tens of μG. This field can be blown over the plane and twisted azimuthally due to the angular momentum conservation, to form an extended magnetized Halo. Using a simple model of such a magnetic field structure, we assess the possible impact of this environment on the interpretation of the arrival directions of incoming Ultra-High Energy Cosmic Rays as a function of rigidity.

38th International Cosmic Ray Conference (ICRC 2023)
July 6th – August 3rd, 2023
Nagoya, Japan

*Speaker

PoS(ICRC2023)320

1. Introduction

There have been several indications that our Galaxy has a nuclear wind. An absence of H I 21cm emission at $|z| > 500$ pc and $R < 3$ kpc from the Galactic center (GC) has been found [1], which is attributed to a clearing of the neutral gas by a nuclear wind. Supporting this possibility, powerful mass ejections from the GC have been observed on scales of several arcminutes to tens of degrees in the infrared, radio, X-rays, and γ-rays [2–4]. Evidence for a large-scale bipolar wind emanating from the GC was found in infrared dust emission by the Midcourse Space Experiment (MSX) [5], suggesting that the GC drives large-scale winds into the halo every $\sim 10 - 15$ Myr.

Hubble Space Telescope (HST) and Far Ultraviolet Spectroscopic Explorer (FUSE) medium resolution spectroscopy along two high-latitude AGN sight lines (Mrk 1383 and PKS 2005–489) above and below the Galactic Center (GC) at $l \sim 0°$ observed four absorption features consistent with a wind emanating from the GC, with velocities of $+250 \pm 20$ km/sec at a height of $|z_{\rm max}| = 12 \pm 1$ kpc above the Galactic plane, implying that they were ejected from the GC at the same speed [6]. These velocities are $\sim 1/2$ of the escape velocity at that position, and therefore they most likely belong to a part of the gas that forms a fountain. Interestingly, their rather low metallicity is inconsistent with a recent ejection, which may indicate that there is also a significant amount of ionized hotter gas that is not visible and could be transferring momentum and structuring a large scale magnetic field in the Halo, even if the wind is gravitationally unbound. In fact, it is possible that the gas associated with the Galactic wind has a temperature $> 10^6$ K. If the dominant wind component is so hot, then the high velocity absorbers would represent cooler material associated with the wind, that is gravitationally bound to the Galaxy, while a dominant hotter and highly-ionized gas could be moving fast enough to produce an unbound wind. Very hot gas associated with the Galaxy has been detected by Chandra in O VII and O VIII in sight lines at Galactic latitudes near the Galactic center (e.g., [7–9]).

A nuclear starburst near our own GC is rendered even more plausible by the discovery of three rich clusters of early-type stars which could account for nearly 10% of all massive stars in our galaxy [[10]]. The Arches Cluster alone, may contain 10^4 $M_\odot$ of stars created in a burst some 2.5 ± 0.5 Myr ago and producing $> 10^{51}$ ionizing ph s^{-1} [11]. There is also abundant evidence that the GC has experienced several starburst periods in the last 20 Myr (see, [11, 12]).

Furthermore, the interpretation of a wind conformed by coexisting phases with different temperatures and filling factors may be strengthened by 3D numerical simulations from [13], in which a highly patchy and filamentary wind can be maintained by Type Ia SNe in the Bulge. The properties of the gas fluctuate in time, particularly in the central region within the sonic radius of the wind, where the discreetness of individual SNe explosions cannot be smooth out in time and space.

The possibility of a Galactic outflow, whether unbound or bound, fountain-like but still reaching large galactocentric distances is strengthened by the observation that other face-on spiral galaxies present spiral magnetic structures in their disk, similar to the Milky Way, showing that our magnetic field is a rather typical feature for such class of galaxies. Furthermore, RM-synthesis of CHANGE-ES observations [14] shows an increasing number of edge-on spiral galaxies presenting X-shaped structures surrounding the disk and extending orderly to distances of up to tens of kpc, increasing the likelihood of a similar large scale magnetic structure in the Galactic Halo. Vertical giant magnetic ropes have also been observed in at least two spiral galaxies. Interestingly, the ordered magnetic

field extend far out into the halo and beyond, and field reversal have been detected in the halo, indicating the possibility that the ropes are tightly bound [14].

All these observations strongly suggest that large outflows of hot plasma do occur in spiral galaxies with varying degrees of star formation rate in their nucleus, resulting in either a bound fountain or an unbound wind. This is frequently associated with large scale structured magnetic fields in their halos. The Milky Way is a rather common spiral with at least episodic star bursts in the center. Therefore, the plausibility of such an outflow and of a corresponding extended structured Halo magnetic field with scales of several kpc merits consideration.

In this proceeding, we will show the impact of such extended regular halo magnetic field on the observation of Ultra-High Energy Cosmic Rays (UHECR) using simulations with a simple model of the Galactic magnetic field.

2. Galactic magnetic field model

If the structure of the magnetic field inside the disk of the Milky Way is largely unclear, the problem becomes even more difficult in the case of the Halo. In this work, we apply the model developed in [15], whose main features are described below.

Following Ref. [16], the Galactic magnetic field $\boldsymbol{B}$ is modeled in terms of a linear superposition of the disk field $\boldsymbol{B}_{\rm disk}$ and the halo field $\boldsymbol{B}_{\rm halo}$:

$$\boldsymbol{B}_{\rm tot} = \boldsymbol{B}_{\rm disk}\,(1 - T(z, z_0)) + \boldsymbol{B}_{\rm halo}\,T(z, z_0)\,, \tag{1}$$

where $T(z, z_0)$ the logistic function

$$T(z, z_0) = \frac{1}{1 + \exp(-k(|z| - z_0))}\,, \tag{2}$$

The growth rate $k = 1/\lambda_{dh}$ determines the steepness of the curve. We set $\lambda_{dh} = 10$ pc, so that $T(z, z_0)$ behaves like a continuous step function, ensuring a smooth transition between both components of the field, with z_0 the midpoint of the (narrow) transition region.

Both $\boldsymbol{B}_{\rm disk}$ and $\boldsymbol{B}_{\rm halo}$ have a regular and a turbulent component. Since the observed Faraday rotations are due to the regular components, although the turbulent is larger, in what follows we will not consider it. The disk field and the halo field are parameterized independently. We use a cylindrical (r, φ, z) coordinate system for the disk and a spherical (ρ, θ, φ) coordinate system for the halo, both with the origin at the Galactic center. These coordinate systems together with the corresponding unit vectors are shown in Fig. 1.

The disk field is parallel to the xy plane and has a shape similar to the spiral structure of the Galaxy. We use the bi-symmetric version of the logarithmic spiral model, with opposite direction of the field in different arms [17] *:

$$\boldsymbol{B}_{\rm disk} = B_{\rm disk}(r, \varphi)\,\left[\sin p\,\boldsymbol{U}_{\rm r} + \cos p\,\boldsymbol{U}_{\phi}\right] \tag{3}$$

The amplitude $B_{disk}(r, \varphi)$ of the disk field at a point (r, φ) of the Galactic plane is given by

$$B_{\rm disk}(r, \varphi) = B_D(r) \cos\left(\phi + b \ln\left(\frac{r}{R_\odot}\right) - \Phi\right), \tag{4}$$

*The sign of the cosine term has been changed compared to [17] according to the definition of our referential having, in particular, the Earth in $x = -8.5$ kpc.

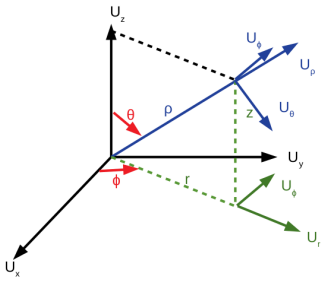

Figure 1: Coordinate systems used to express the magnetic fields of the disk (r, φ, z) and the halo (ρ, φ, θ).

where $r_\odot$ is the Galactocentric distance of the Sun, taken as 8.5 kpc, and

$$b = \frac{1}{\tan p}\,, \qquad \Phi = b \ln\left(1 + \frac{d}{r_\odot}\right) + \frac{\pi}{2}\,. \tag{5}$$

Here, d is the distance for the first field reversal, p is the pitch angle, and

$$B_D(r) = \frac{B_0^d}{\cos\Phi} \begin{cases} r_\odot / r_c\,, & r < r_c \\ r_\odot / r\,, & r \geq r_c \end{cases} \tag{6}$$

where B_0^d is the local field intensity at the Sun's position and r_c is the characteristic radius of the central region where the field is assumed to be constant ($r_c \geq 1$ kpc).

Regarding the halo field, we assume that it is composed of an X-shape field and a toroidal field [16, 18]. We model it with an Archimedean spiral [19], consistent with a large-scale magnetic field due to winds, which in spherical coordinates is defined as:

$$\boldsymbol{B}_{\rm halo} = \frac{|z|}{z}\, B_0^h \left(\frac{\rho_0}{\rho}\right)^2 \left[\boldsymbol{U}_\rho + \frac{\rho}{\rho_1} \sin\theta\, \boldsymbol{U}_\phi\right] \tag{7}$$

with ρ_1 the typical distance where the halo field changes from radial to azimuthal and B_0^h denotes the magnetic field strength, ρ_0 is the spherical radius at which B_0^h is defined, and the factor $|z|/z$ accounts for the reversal of the field direction: up above and down below the Galactic plane, which reproduces the dipole structure observed with Faraday measurements. The lines leave the origin in the north hemisphere and re-enter from below in the south hemisphere. The field rotates clockwise instead of anti-clockwise above the disk (this is equivalent to take ω negative in [19]).

In the rest of the proceeding we will use the best parametrization obtained in [15]. The projections of this best field are represented on Fig. 2.

3. Effect of halo magnetic field on backtracking of Ultra-High Energy Cosmic Rays

3.1 Method

To emphasise the impact of the halo magnetic field on the arrival direction of UHECR, we have backtracked antiprotons in a circle of 1° around a central position up to 20 kpc. This aims to reproduce the uncertainty on the arrival of a particular cosmic ray. As an illustration, in Fig. 3

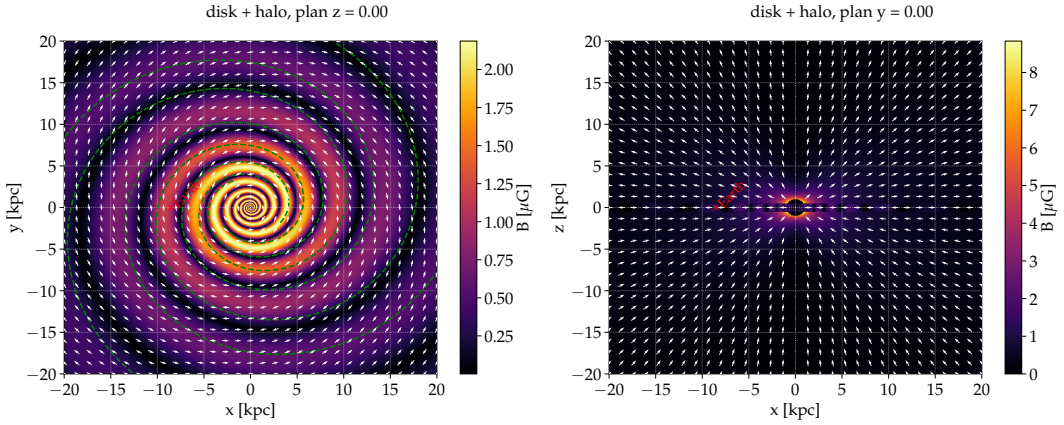

Figure 2: Map ($z = 0$ and $y = 0$) of the magnetic field for the best fit. As matter of comparison, on the $z = 0$ plane we represented the spiral arms as computed in NE2001 with green dashed lines.

the results of the backtracking for six randomly selected positions in the sky are shown. In grey is represented the area of injection of the antiprotons. The coloured areas depict the arrival position at the border of the Galaxy for three rigidities (red: 10^{20} eV, green: 10^{19} eV, blue: $10^{18.5}$ eV). Skymaps has been made for the disk magnetic field only (left) and for the disk + halo magnetic field (right).

These maps can be interpreted in two ways. A cosmic ray with a given rigidity that arrives at the edge of the Galaxy in a colored region, will be observed at Earth in the corresponding grey area (markers placed to keep track of the backtracking). Conversely, a cosmic ray observed on Earth in any of the grey regions with a certain rigidity arrived from their source at the edge of the Galaxy in the corresponding colored area. If we assume that, on its journey to the Milky Way, the particle did not interact in the intergalactic medium (no photo-pion production or photo-disintegration) and was not deflected by any ambient intergalactic field, then the colored areas correspond to the regions where to look for its source. Of course, this is a strong assumption, especially for low-energy events that could be secondary particles produced by the interaction of higher-energy primaries with photons of the cosmic microwave background. Nevertheless, by way of illustration, we have placed orange stars to highlight the position of the brightest active galactic nuclei and star-burst galaxies that are candidates as possible sources of UHECR.

Qualitatively, we can already draw some conclusions. For the situation with only the disk magnetic field (left map in Fig. 3), the impact is moderate, especially for the high rigidity events (red and green), which hardly deviate at all. Low rigidity events (blue) only deviate by a few degrees. The shape of the uncertainty region is very little affected and remains nearly circular. In contrast, when we add the halo component (right map), more complex behaviors can occur. Except for the events with the highest rigidity (red), which deviate slightly, the intermediate (green) and low (blue) rigidity events deviate by more than 20°. Moreover, the shape of the search region at the edge of the Galaxy can be deformed considerably, as shown by the blue regions. Finally, in general, we can observe an alignment of the regions following the rigidity. But the "square" event ($l \sim 70°$, $b \sim 25°$) and the the "diamond" event ($l \sim 60°$, $b \sim -5°$) show that more complex behaviors can occur. The search regions for the three rigidities lead to very different regions in the sky that are

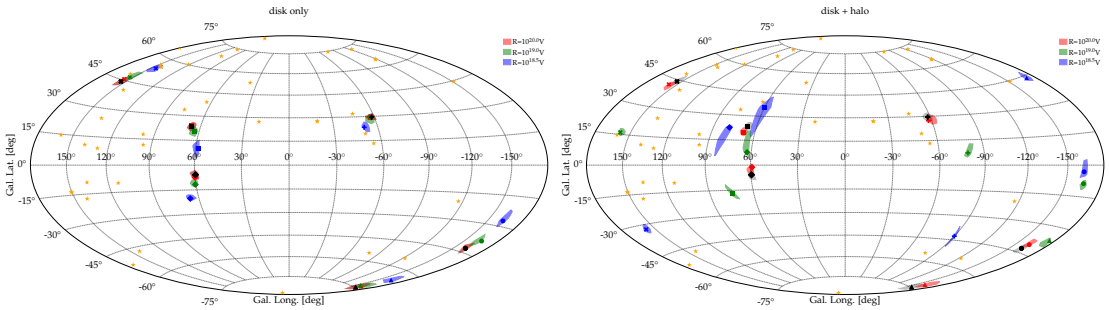

Figure 3: Backtracking of cosmic rays for 6 positions in the sky (black dots) and three rigidities. 100 antiprotons for each rigidity were injected in the grey area ($\sim 1°$) around each black dot, giving the corresponding colored areas (red, green, and blue) at the arrival positions. On the left, a disk-only model for the Galactic magnetic field and, on the right, a disk + halo model.

not a priori linked on a first interpretation. This means that two UHECR observed very close but with slightly different rigidity, which could supposedly be associated are actually coming from two different sources.

3.2 Full sky effect

To quantitatively estimate the halo effect on the observations of UHECR with more than a few positions, we have reproduced the previous backtracking of 100 antiprotons for 2000 initial central positions of observation randomly distributed (uniform distribution) in the sky. Two parameters have been chosen to quantify the effect: the average angular distance $\langle D_i \rangle$ between the initial position of backtracking and its arrival position on the edge of the Galaxy and the maximal angular distance ($\max(L_i)$) between the 100 positions after backtracking for each of the 2000 positions. In Fig. 4 (left) is represented the frequency of obtaining a certain average deflection angle for the two Galactic magnetic field models: without halo magnetic field (dashed lines) and with it (plain lines) and for the three rigidities previously used (same colour code). The dashed lines clearly show that what is observed for few positions on the skymap without halo field (Fig. 3 left) is valid for any position on the sky. At the highest rigidities, the effect of only the disk magnetic field is almost ineffective to change the arrival directions. For the lowest rigidity, most deflections are lower than $20°$. Instead, adding an extended halo magnetic field, even on short distances, has a large impact. Intermediate rigidities (green) are mostly deflected $\sim 30°$ from the source and low rigidities (blue) can be deflected from 0 to more than $100°$, with the deviations being totally dependent on the position of the source in the sky. On Fig. 4 (right) is represented $\max(L_i)$. This parameter gives a rough estimation of how much the search region for a cosmic ray is deformed. Of course, we should remember that the deformation can be very different from one case to another (see Fig. 3) and, therefore, what is plotted there represents only a global behaviour. Typically, as for the average deflection angle, what is shown on the skymaps is confirmed. There is no excessive deformation coming from the disk magnetic field alone for any rigidity. Instead, adding the halo magnetic field creates larger deformations as the rigidity decreases.

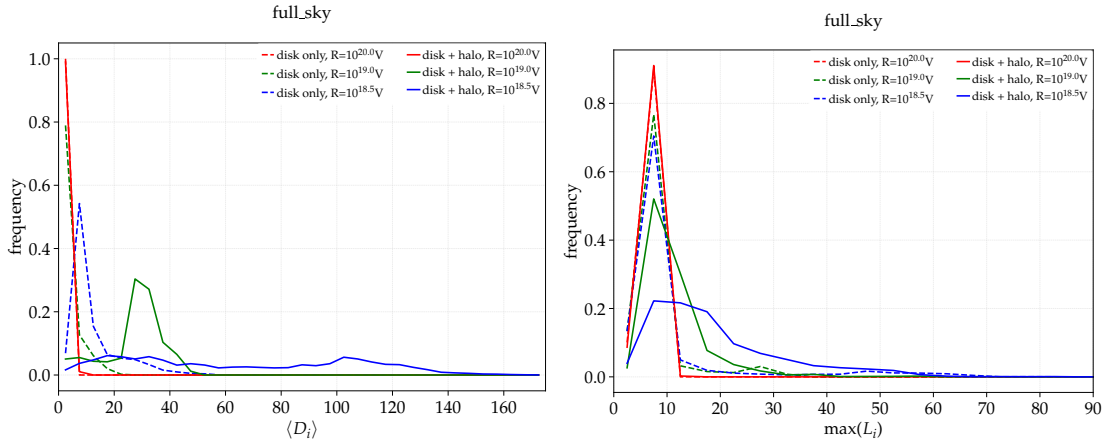

Figure 4: Frequency of average deflection angle $\langle D_i \rangle$ and maximal extension L_i of the backtracking of a 2000 1° angle region randomly located on the sky.

3.3 Case study: a Centaurus A hotspot

To highlight the importance of the halo magnetic filed in the search for the origin of UHECR, we will conclude this proceeding with a short case study. Following the same procedure as previously, we focus on events located in a "hotspot" of 30° around Centaurus A. In Fig. 5 is represented in grey an observed "hotspot" on Earth. Like on Fig. 3, each colored area represents the search region on the edge of the Galaxy for three rigidities (red: 10^{20} eV, green: 10^{19} eV, and blue: $10^{18.5}$ eV). In the skymap on the left, only the disk magnetic field is considered, while in the one on the right, both the magnetic field of the disk and the halo are taken into account. When only the disk magnetic field is considered, the search region of the "hotspot" source is not affected for the highest rigidities (red and green) and barely for the lowest rigidity (blue). The orange stars representing the most active AGNs and SBGs inside the four regions are the same: Centaurus A, M83, NGC4945, AP Librae, and Mkn180. Thus, the search for sources should not be greatly affected by deflections due to the disk magnetic field. In contrast, by adding the halo magnetic field, while the highest rigidity search region (red) is almost unaffected, the intermediate region (green) moves west and extends to the south and north, and the lowest (blue) becomes noticeably larger and moves to the southern hemisphere, including new sources for the search.

4. Conclusions

This brief study, even with limited modeling of the galactic magnetic field, has allowed us to highlight the important impact that an extended halo can have on the interpretation of the direction of arrival of Ultra-High Energy Cosmic Rays and the search for their sources. If we include a mixed composition of cosmic rays at the highest energy, then the image in rigidity becomes even more complex. Two nearby particles with the same energy but of a different nature could be misinterpreted as originating from the same source.

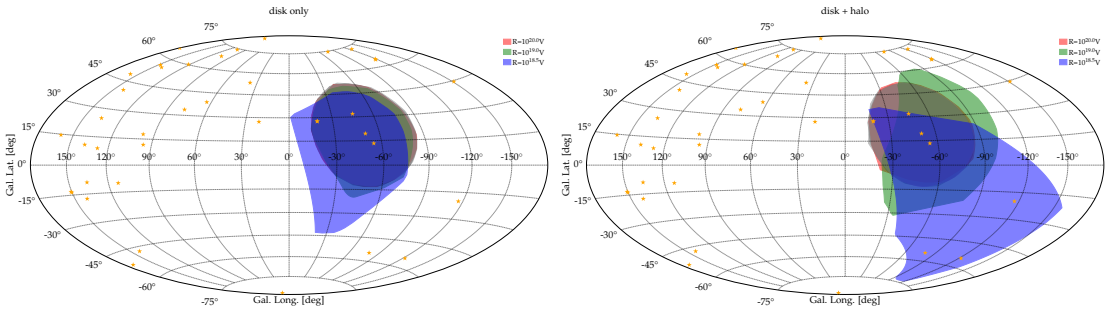

Figure 5: Backtracking of cosmic rays of a Centaurus A "hotspot" of 30° three rigidities (colours). 2000 antiprotons for each rigidity were injected in the grey area. On left disk only model of for the Galactic magnetic field and on right disk + halo.

References

[1] F.J. Lockman, *The Astrophysical Journal* **283** (1984) 90.

[2] M. Morris and E. Serabyn, *Annual Review of Astronomy and Astrophysics* **34** (1996) 645.

[3] L.X. Cheng, M. Leventhal, D.M. Smith, W.R. Purcell, J. Tueller, A. Connors et al., *The Astrophysical Journal* **481** (1997) L43.

[4] F. Yusef-Zadeh, F. Melia and M. Wardle, *Science* **287** (2000) 85.

[5] J. Bland-Hawthorn and M. Cohen, *The Astrophysical Journal* **582** (2003) 246.

[6] B.A. Keeney, C.W. Danforth, J.T. Stocke, S.V. Penton, J.M. Shull and K.R. Sembach, *The Astrophysical Journal* **646** (2006) 951.

[7] A. Rasmussen, S.M. Kahn and F. Paerels, in *The IGM/Galaxy Connection: The Distribution of Baryons at z=0*, J.L. Rosenberg and M.E. Putman, eds., (Dordrecht), pp. 109–116, Springer Netherlands (2003), DOI.

[8] F. Nicastro, S. Mathur, M. Elvis, J. Drake, F. Fiore, T. Fang et al., *The Astrophysical Journal* **629** (2005) 700.

[9] B. McKernan, T. Yaqoob and C.S. Reynolds, *Monthly Notices of the Royal Astronomical Society* **361** (2005) 1337.

[10] D.F. Figer, *Symposium - International Astronomical Union* **212** (2003) 487.

[11] D.F. Figer, F. Najarro, D. Gilmore, M. Morris, S.S. Kim, E. Serabyn et al., *The Astrophysical Journal* **581** (2002) 258.

[12] S. Veilleux, G. Cecil and J. Bland-Hawthorn, *Annual Review of Astronomy and Astrophysics* **43** (2005) 769.

[13] S. Tang, Q.D. Wang, M.-M. Mac Low and M.R. Joung, *Monthly Notices of the Royal Astronomical Society* **398** (2009) 1468.

[14] M. Krause, J. Irwin, P. Schmidt, Y. Stein, A. Miskolczi, S.C. Mora-Partiarroyo et al., *arXiv e-prints* **2004** (2020) arXiv:2004.14383.

[15] T. Fitoussi, G. Medina-Tanco and J.-C. D'Olivo, vol. 395, p. 451, SISSA Medialab, Mar., 2022, DOI.

[16] R. Jansson and G.R. Farrar, *The Astrophysical Journal* **757** (2012) 14.

[17] M.S. Pshirkov, P.G. Tinyakov, P.P. Kronberg and K.J. Newton-McGee, *The Astrophysical Journal* **738** (2011) 192.

[18] P. Terral and K. Ferrière, *Astronomy and Astrophysics* **600** (2017) A29.

[19] E.N. Parker, *The Astrophysical Journal* **128** (1958) 664.

PoS(ICRC2023)320